

1 **Does consideration of water routing affect simulated water and carbon dynamics in**
2 **terrestrial ecosystems?**

3 G. Tang^{†,1}, T. Hwang², and S.M. Pradhanang³

4

5 ¹Division of Earth and Ecosystem Sciences, Desert Research Institute, Reno, NV, USA

6 ²Institute for the Environment, University of North Carolina, Chapel Hill, NC, USA

7 ³Institute for Sustainable Cities, City University of New York, New York, NY, USA

8

9 ¹Contact information for the corresponding author:

10 Dr. Guoping Tang

11 Division of Earth and Ecosystem Sciences

12 Desert Research Institute

13 2215 Raggio Parkway

14 Reno, NV 89512

15 USA

16 Phone (775) 673-7938; Fax (775) 673-7485

17 Email: tangg2010@gmail.com

18 **Abstract:** The cycling of carbon (C) in terrestrial ecosystems is closely coupled with the cycling
19 of water. An important mechanism connecting ecological and hydrological processes in
20 terrestrial ecosystems is lateral flow of water along landscapes. Few studies, however, have
21 examined explicitly how consideration of water routing affects simulated water and C dynamics
22 in terrestrial ecosystems. The objective of this study is to explore how consideration of water
23 routing in a process-based hydro-ecological model affects simulated water and C dynamics. To
24 achieve that end, we rasterized the regional hydroecological simulation system (RHESSys) and
25 employed the rasterized RHESSys (R-RHESSys) in a forested watershed. We performed and
26 compared two contrasting simulations, one with and another without water routing. We found
27 that R-RHESSys was able to correctly simulate major hydrological and ecological variables
28 regardless of whether water routing is considered. When water routing was considered, however,
29 soil water table depth and saturation deficit were simulated to be greater and spatially more
30 heterogeneous. As a result, water (evaporation, transpiration, and evapotranspiration) and C
31 (forest productivity, soil autotrophic and heterotrophic respiration) fluxes also were simulated to
32 be spatially more heterogeneous compared to the simulation without water routing. When
33 averaged for the entire watershed, the three simulated water fluxes were greater while C fluxes
34 were smaller under simulation considering water routing than that ignoring water routing. In
35 addition, the effects of consideration of water routing on simulated C and water dynamics were
36 more apparent in dry conditions. Overall, the study demonstrated that consideration of water
37 routing enabled R-RHESSys to better capture our preconception of the spatial patterns of water
38 table depth and saturation deficit across the watershed. Because soil moisture is fundamental to
39 the exchange of water and C fluxes among soil, vegetation and the atmosphere, ecosystem and C

40 cycle models, therefore, need to explicitly represent water routing in order to accurately quantify
41 the magnitude and patterns of water and C fluxes in terrestrial ecosystems.

42 **Keywords:** R-RHESSys, carbon cycle, water, lateral flow, hydrologic connectivity, watershed

43 **1. Introduction**

44 The cycling of carbon (C) in terrestrial ecosystems is closely coupled with the cycling of
45 water. Plants need water to survive, and thus, the distribution, composition, and structure of plant
46 communities are directly influenced by spatial patterns of available water (Band, 1993; Band et
47 al., 1993; Caylor et al., 2005; Ivanov et al., 2008). An important mechanism that connects
48 ecological and hydrological processes in terrestrial ecosystems is lateral water flow along
49 landscapes. Lateral water flow can redistribute water and nutrients through space, which affects
50 plant establishment and growth (Band et al., 1993) ; leaf phenology (Asbjornsen et al., 2011);
51 ecosystem structure and function (Wang et al., 2009); and soil biogeochemical processes, such as
52 organic matter decomposition (Ju et al., 2006; Riveros-Iregui et al., 2011). For example, studies
53 have demonstrated that lateral water flow and connectivity act as important determinants of
54 ecological pattern and process in heterogeneous landscapes (Band et al., 1993; Sponseller and
55 Fisher, 2008), and contribute to changes in surface water, energy, nutrients, and C in space
56 (Pockman and Small, 2010). In mountainous catchments, Hwang et al. (2012) found that lateral
57 water flow can produce important patterns in water and nutrient fluxes as well as stores, which
58 influences the long-term spatial development of forest ecosystems. Riveros-Iregui et al. (2011)
59 suggested that landscape-imposed redistribution of soil water is a major cause for distinct
60 variation of growing season soil CO₂ efflux within small subalpine watersheds.

61 Hydrological connectivity via lateral water flow plays important roles in the transport of
62 water, nutrients and sediments at catchment scales (Smith et al., 2010). Correspondingly,
63 distributed hydrology models (DHM) that simulate lateral water flow and its spatial connectivity
64 along landscapes or among simulated grids have been developed increasingly in recent years
65 (Lane et al., 2009). These models – such as DHSVM (Wigmosta et al., 1994) and RHESSys

66 (Band et al., 1993; Tague and Band, 2004) – couple runoff generation and water routing
67 mechanisms and thus are able to explicitly simulate the effects of topographic and subsurface
68 heterogeneities on downslope redistribution of water and nutrients (Doten et al., 2006). In fact,
69 DHMs are used widely to identify saturated areas that produce runoff and non-point source
70 pollution (Gerard-Marchanti et al., 2006), evaluate irrigation systems (Singh et al., 2006), and
71 examine flood potential associated with disturbances such as deforestation (Doten et al., 2006).
72 The representation of soil moisture variability and water routing processes at grid cell level in
73 DHMs also enables these models to account for spatial variability of runoff-generating
74 mechanisms and infer model parameterization from distributed geospatial data such as geology,
75 topography, soils, and land cover (Wang et al., 2011). These advantages greatly contributed to
76 the accuracy of hydrologic forecasting (Smith et al., 2012).

77 Despite the fact that lateral water flow redistributes water and nutrients in space and thus
78 affects ecosystem structure and function as well as the cycling of water and C, the representation
79 of lateral water flow and its spatial connectivity may not be adequate in existing ecosystem and
80 C cycle models. For example, Riveros-Iregui et al. (2011) indicated that the robust
81 implementation of the lateral redistribution of soil water into biogeochemical models is often
82 lacking. Chen et al. (2005) argued that most C cycle models at regional and global scales use
83 bucket models to estimate soil moisture and ignore lateral exchanges of water among simulated
84 units. The causes for such inadequacy are (i) lack of detailed information on how lateral water
85 flow may affect vegetation, water, and C dynamics in terrestrial ecosystems, and (ii) increased
86 burden of computing when water routing is included in the model's simulation (Ju et al., 2006;
87 Zhou et al., 2010). This inadequacy, however, is likely to hinder better quantification of the

88 spatial heterogeneity and complex linkages of hydrological, ecological, and biogeochemical
89 processes in terrestrial ecosystems.

90 Furthermore, mountain forests account for about 23% of the Earth's forest cover and play an
91 important role in modulating global cycling of water and C (Price et al., 2011). Given the
92 elevational gradient in mountain forests plus gravity, lateral water flow – such as subsurface
93 lateral flow along slopes – is common in humid mountain forests (Ridolfi et al., 2003). In semi-
94 arid and arid ecosystems, surface lateral flow also occurs when rainfall intensity exceeds the
95 infiltration capacity of dry soils (Kim and Eltahir, 2004) or on topographically flat ground if the
96 presence of the vegetation patch creates a contrast in infiltration rate (Thomson et al., 2011).
97 The universality and significance of lateral water flow in terrestrial ecosystems suggest that it
98 should not be overlooked by ecosystem and C cycle models. A better understanding of how
99 lateral water flow and its spatial connectivity may affect water and C dynamics is therefore
100 important for accurate quantification of terrestrial water and C budgets as well as sustainable
101 management of water and forest resources (e.g., Wang et al., 2011).

102 The overall objectives of this study are to investigate (i) how consideration of water routing
103 in a process-based, hydro-ecological model affects simulated water and C dynamics in terrestrial
104 ecosystems; and (ii) if effects of consideration of water routing on simulated C and water
105 dynamics are more remarkable in dry conditions. Toward these ends, we rasterized a regional
106 hydro-ecological model designed to simulate integrated water, C and nutrient dynamics at
107 watershed and regional scales. The rasterization aimed to (i) remove the model's hierarchical
108 structure so that all hydrological and ecological processes would be simulated at the individual
109 cell level; and (ii) add a new control interface so that the water routing algorithm built into the
110 model could be switched on or off. These modifications allowed us to keep all model parameters

111 and their parameterization identical between two predesigned contrasting simulations: with vs.
112 without water routing. In turn, this helped reduce the uncertainty of model-based comparisons
113 that can result from differences in model structure, parameters, and parameterization – as
114 commonly encountered in model-based inter-comparison studies. Based on the rasterized model,
115 we performed the two contrasting simulation for each of two contrasting forcing scenarios: “wet”
116 vs. “dry” scenario. We compared simulated soil water table depth and saturation deficit,
117 evaporation, transpiration, evapotranspiration, forest productivity, and soil respiration from these
118 simulations. Findings gained from these comparisons provide insights into the future
119 development of ecosystem and C cycle models for terrestrial ecosystems.

120 **2. Material and Data**

121 **2.1 Study area**

122 The Biscuit Brook (hereafter Biscuit) watershed in the Catskill Mountain Region of New
123 York State (Fig. 1) was selected as the study region. This watershed is relatively humid with
124 annual total precipitation of about 145 cm and annual mean temperature about 4.4 °C. The slopes
125 vary from 0.04° to 37°, and the maximum slope length is 4.73 km in a northeast to southwest
126 direction (Fig. 1). We selected this watershed as the study region because (i) long-term historical
127 streamflow observations from one USGS gauge station (01434025) for this watershed are
128 available to calibrate and evaluate model simulations; (ii) this watershed is forested and thus well
129 suited for investigating the linkages between ecological and hydrological processes; (iii) there
130 are no human-related land use activities; and (iv) the watershed has spatially variable terrain with
131 elevation ranging from 270 to 1270 m, providing a natural hydro-ecological laboratory to
132 examine the effects of lateral water flow and its spatial connectivity on water, C and vegetation
133 dynamics in terrestrial ecosystems.

134 **2.2 Rasterizing the Regional Hydro-Ecological Simulation System**

135 The Regional Hydroecological Simulation System (RHESSys, Tague and Band (2004)) is a
136 process-based hydro-ecological model designed for simulating integrated water, C and nutrient
137 dynamics as well as vegetation growth at watershed and regional scales. Although RHESSys is
138 capable of being run in fully distributed mode, its hierarchical framework requires that some
139 initial-state variables associated with the spatial hierarchy of basins, hillslopes, and zones be
140 arranged per a prescribed template. In this study, we further rasterized RHESSys (version 5.12)
141 in an attempt to remove the model's hierarchical structure. The rasterized RHESSys (hereafter R-
142 RHESSys) adopted almost all features of its predecessor except for (i) exclusion of the
143 hierarchical model framework of RHESSys, and (ii) modification of the user-interface for
144 controlling model simulation. The exclusion of the hierarchical structure in R-RHESSys caused
145 the basin, hillslope, and zone hierarchical structures existing in RHESSys to exist no longer. As a
146 result, arrangement of some initial-state variables according to the prescribed template (i.e., the
147 World file in RHESSys) was no longer needed. In addition, R-RHESSys excluded the
148 TOPMODEL (Beven and Kirkby, 1979) embedded in its predecessor but retained the explicit
149 water-routing algorithm (Wigmosta et al., 1994) for simulating surface and subsurface lateral
150 flow as well as movement of solutes through space. The water routing algorithm in R-RHESSys
151 can be switched on or off and thus provides users two ways (i.e., with vs. without water routing)
152 to quantify C, water, and nutrient dynamics in terrestrial ecosystems. As in its predecessor,
153 surface and subsurface lateral flow for stream-type patches are channelized in R-RHESSys.

154 Because specific algorithms for C, water, and nutrient dynamics are maintained mostly as in
155 Tague and Band (2004), we briefly introduced calculation of subsurface and surface flow that

156 was slightly modified for reference. In R-RHESSys, the saturated subsurface flow ($SF_{a \rightarrow b}$) (m
 157 day⁻¹) from patch a to b is calculated as follows:

$$158 \quad SF_{a \rightarrow b} = \begin{cases} \delta \times \gamma \times (e^{-s/m} - e^{-s_{\max}/m}) & s \geq 0 \\ \delta \times \gamma \times (e^{-s/(3.5 \times m)} - e^{-s_{\max}/m}) & s < 0 \end{cases} \quad (1)$$

159 where, s (m) is saturation deficit in patch a ; m (dimensionless) is the decay rate of soil hydraulic
 160 conductivity with depth in patch a ; s_{\max} (m) is the water equivalent of soil depth; δ
 161 (dimensionless) is the empirical sensitivity parameter with a value of 1.2 when water routing is
 162 considered and a value of 0.16 when water routing is ignored. The values 1.2 and 0.16 are based
 163 on model calibrations (see below); and γ (m day⁻¹) is the percent of subsurface flow going from
 164 patch a to patch b . It is expressed as:

$$165 \quad \gamma = K_{sat0} \times \tan \beta_{a \rightarrow b} \times W_{a \rightarrow b} \quad (2)$$

166 where K_{sat0} (m day⁻¹) is saturated hydraulic conductivity at the surface; β (degree) is the local
 167 slope from patch a to patch b ; and W (dimensionless) is the flow width from patch a to patch b .
 168 The flow widths are assumed to be 0.5 times the grid size for cardinal directions and 0.354 times
 169 the grid size for diagonal directions (Quinn et al., 1991; Tague and Band, 2004).

170 The saturation overland flow (RF_a) for patch a is expressed as follows:

$$171 \quad RF_a = \max(RS + UsatS - s, 0.0) \quad (3)$$

172 where RS (m) is soil water storage in the root zone layer; and $UsatS$ (m) is soil water storage in
 173 the un-saturated soil layer.

174 When water routing is considered in R-RHESSys, the saturated subsurface flow input from
 175 the upslope patch a (Eq. 1) is added to the downslope patch b and accounted for in patch b 's
 176 local water budget. When routing is turned off, Eq. 1 is still used to calculate subsurface flow out
 177 of each patch. However, rather than being routed to downslope patches the subsurface outflows

178 from all patches are summed and assumed to flow out of the basin as the baseflow component of
179 streamflow. The value of the sensitivity parameter δ in Eq. 1 for the non-routing case is reduced
180 to reflect the change in function of this parameter from a lateral flow between patches adjustment
181 to what is effectively a baseflow recession coefficient. The other difference between routing and
182 non-routing is that with routing on surface runoff generated by Eq.3 is routed following the same
183 topology as subsurface flow and is allowed to re-infiltrate along its flowpath, whereas with no
184 routing the surface runoff generated by Eq. 3 for all patches is summed and assumed to flow out
185 of the basin as the runoff component of streamflow.

186 **2.3 Meteorological data**

187 Time series of daily maximum and minimum temperature ($^{\circ}\text{C}$) as well as total precipitation
188 (mm) are required to run R-RHESSys. Because there is no weather station located in the Biscuit
189 watershed, our climate data for the period 1961–2008, a period having as long as possible
190 available climate records and preselected for model spin-up simulation, were derived from ten
191 Cooperative Observer Program stations (COOP) (Fig. 1). Specifically, daily climate data for
192 each day in each year for the watershed were estimated using the ordinary-Kriging interpolation
193 approach (Goovaerts, 1998). Before interpolation, daily records of temperatures that exceeded
194 the long-term (1961 – 2008) mean of all available records from that station by four standard
195 deviations or greater were manually removed on a case-by-case basis (e.g., Tang and Arnone,
196 2013). In addition, local lapse rates of $-0.0085\text{ }^{\circ}\text{C m}^{-1}$ for daily maximum temperature, -0.0054
197 $^{\circ}\text{C m}^{-1}$ for daily minimum temperature, and 0.0014 mm m^{-1} for daily precipitation were used to
198 adjust temperature and orographic precipitation changes along the elevation gradient in the study
199 sites. Figure A1 in supplementary materials shows examples of interpolated daily maximum and
200 minimum temperatures as well as precipitation for the Biscuit watershed in July, 1994.

201 **2.4 Land cover, soil and elevation data**

202 The land cover data used to pre-define vegetation types for the Biscuit watershed were based
203 on the 1992 National Land Cover Data (NLCD 1992; http://landcover.usgs.gov/us_map.php).
204 The NLCD 1992 data were derived from Landsat Thematic Mapper satellite data at 30-m spatial
205 resolution and classified land covers into 21 types for the United States (Vogelmann et al., 1998a,
206 b). For the Biscuit watershed, only three types exist in NLCD 1992: evergreen, deciduous and
207 mixed forests. Our soil texture data at 30 m spatial resolution were derived from the digital Soil
208 Survey Geographic Database (<http://soils.usda.gov/>). We classified soil in the Biscuit watershed
209 into four types: sandy loam, loamy skeleton, silt loam and rocky (Fig. A1d). Soil texture related
210 parameters and their parameterization are in Table 1. The USGS National Elevation Dataset at 1
211 arc-second spatial resolution (about 30 meters) was used in this study.

212 **2.5 Modeling protocol, model simulation, calibration, and evaluation**

213 Given that climate in the Biscuit watershed is relatively humid and precipitation has no
214 distinct dry and wet cycles, we performed four simulations under two climate forcing scenarios:
215 one “wet” and another “dry” scenario. Under the “wet” scenario, time-series of daily climate data
216 for the period 1961–2008 were directly used without modification. Under the “dry” scenario, we
217 set time-series of daily precipitations for days in May, June, July and August in 1995 all zeroes
218 while keeping others identical to those under the “wet” scenario. For each of the two scenarios,
219 the two contrasting simulations (i.e., with vs. without water routing) were performed,
220 respectively.

221 Our initial simulations under the “wet” scenario suggested that soil water table depth, leaf
222 area index (LAI) and forest productivity tended to reach the equilibrium state after 50
223 simulation-years. In contrast, soil C took more than 200 simulation-years to reach the

224 equilibrium state (Fig. A2). In order to have vegetation and soil C reach equilibrium state with
225 long-term local climate, we spun up R-RHESSys for 240 years repeatedly using 48-year (1961–
226 2008) daily-step meteorological data. After spin-up simulations, we continued to run R-
227 RHESSys for an additional 48 years using data from 1961 to 2008. This modeling protocol
228 applied to all four simulations under both “wet” and “dry” forcing scenarios.

229 Based on results under the “wet” scenario, we calibrated R-RHESSys for the period 1992–
230 1993 and evaluated it for the period 1994–1995. The period 1992–1995 was selected because
231 observed climate records in this period from 10 COOP stations were more consistent than during
232 other periods. This can minimize the effects of the quality of atmospheric forcing data on
233 simulated water and C dynamics. Correspondingly, model calibration and evaluation for each of
234 the two pre-specified periods were performed for the two contrasting simulations under the “wet”
235 scenario, respectively.

236 To investigate how consideration of water routing may affect simulated C and water
237 dynamics, monthly average daily values of major hydro-ecological variables in July of 1994
238 from the two contrasting simulations under the “wet” scenario were compared. The July of 1994
239 was selected because temperature in July is generally higher than in other months and thus the
240 effects of consideration of water routing on simulated water and C dynamics as well as
241 vegetation growth were assumed to be more detectable. To test if effects of consideration of
242 water routing on simulated C and water dynamics are more remarkable in dry conditions, we
243 compared the differences in simulated monthly values of major hydro-ecological variables in
244 1995 between the “wet” and “dry” scenarios.

245 **3. Results**

246 **3.1 Calibration and evaluation of simulated streamflow and baseflow**

247 Fig. 2 shows the time-series of simulated daily streamflow and baseflow for the Biscuit
248 Brook in the watershed for the calibration period 1992–1993 and the evaluation period 1994–
249 1995. For the calibration period, the calculated Nash-Sutcliffe coefficients (NS; Nash and
250 Sutcliffe, 1970) is 0.58 for streamflow (Fig. 2a) and 0.63 for baseflow (Fig. 2b) under the
251 simulation that considered water routing. In contrast, the calculated NS is 0.61 for streamflow
252 (Fig. 2c) and 0.74 for baseflow (Fig. 2d) for the simulation that neglected water routing. For the
253 evaluation period, the calculated NS was more than 0.57 for both streamflow and baseflow
254 regardless of whether or not water routing was considered (Fig. 2a~d). In addition, the simulated
255 average daily streamflow for the evaluation period 1994–1995 approximated each other between
256 the two simulations (2.54 vs. 2.50 mm day⁻¹). The difference in average daily streamflow
257 between model simulations and observation was less than 1.25% under both simulations. These
258 statistics (Table S1) suggested that R-RHESSys was able to accurately simulate daily streamflow
259 and baseflow regardless of whether water routing was considered.

260 **3.2 Comparison of simulated soil water table depth and saturation deficit**

261 When water routing was considered, the simulated depth to the soil water table ranged from
262 0.15 to 2.92 m among cells and averaged 1.20 m for the entire watershed. In contrast, when
263 water routing was ignored, the simulated depth ranged from 0.02 to 1.20 m among cells, and
264 averaged 0.72 m for the entire watershed. In other words, the simulated water table depth was
265 spatially more variable when water routing was simulated as indicated by the calculated standard
266 deviations for soil water table depth among cells (Table 2 and Fig. 3a vs. 3b). A similar situation
267 applied to the simulated saturation deficit, which had a wider range from 0.08 to 1.42 m under
268 simulation with water routing but a narrower range from 0.01 to 0.54 m under simulation without
269 water routing (Table 2). The simulated saturation deficit also was spatially more variable under

270 simulation with water routing than that without water routing (Fig. 3d vs. 3e), as indicated by the
271 standard deviations for saturation deficit among cells (Table 2). Further comparison suggested
272 that water table depth and saturation deficit were about 0.5 m (for water table) and 0.2 m (for
273 saturation deficit) greater in the hills or ridges of the watershed when water routing was
274 considered. In the valleys or flat areas, however, there are regions where the simulated water
275 table depth and saturation deficit were smaller when water routing was considered compared to
276 the simulation ignoring water routing (Fig. 3c and 3f). Spatially, deeper water table depth and
277 higher saturation deficit were simulated to occur mostly at upslope areas (Fig. 3a and 3d) when
278 water routing was considered. This situation, however, did not always apply to simulations
279 ignoring water routing, under which water table depth and saturation deficit were found to be
280 greater at steeper slopes (Fig. 3b and 3e).

281 **3.3 Comparison of simulated evaporation, transpiration, and evapotranspiration**

282 Compared to the simulation ignoring water routing, simulated monthly average daily
283 evaporation, transpiration, and actual evapotranspiration (ET) with water routing had a wider
284 range among cells. For example, monthly average daily evaporation for July 1994 was simulated
285 to vary from 0.22 to 3.11 mm day⁻¹ among cells under simulation with water routing. In contrast,
286 evaporation had a narrower range from 0.52 to 1.05 mm day⁻¹ under the simulation without water
287 routing (Table 2). When averaged for the entire watershed, monthly average daily evaporation,
288 plant transpiration, and ET were 18% (0.87 vs. 0.74 mm), 4% (1.41 vs. 1.35 mm) and 9% (2.27
289 vs. 2.09 mm) greater, respectively, under simulation considering water routing than that ignoring
290 water routing (Table 2). In addition, regardless of the actual magnitudes of simulated water
291 fluxes, the spatial patterns of evaporation, transpiration, and ET were modeled to be more
292 variable under simulation considering water routing than that ignoring water routing, largely

293 because extreme high and low values of evaporation, transpiration and ET were simulated to
294 occur under the simulation with water routing (Figs. A3 and 4). Spatially, the effects of
295 considering water routing on simulated evaporation, transpiration, and ET can be either positive
296 or negative compared to the simulation neglecting water routing (Fig. A3).

297 **3.4 Comparison of simulated forest net primary productivity (NPP)**

298 At the individual cell level, simulated monthly average daily NPP in July, 1994 when
299 ignoring water routing ranged from 2.50 to 5.79 gC m⁻², narrower than results from the
300 simulation considering water routing which ranged from 0.10 to 5.79 gC m⁻² among cells. In
301 addition, although the pattern of simulated NPP was extremely similar in most areas of the
302 watershed between the two simulations (Fig. 5a and 5b), simulated monthly average daily NPP
303 among cells was spatially more variable when water routing was considered, as suggested by the
304 calculated standard deviations for NPP among cells (Table 2). When averaged for the entire
305 watershed, the simulated monthly average daily NPP was 8% (3.33 vs. 3.60 gC m⁻²) lower under
306 simulation considering water routing than that ignoring water routing (Table 2). Nevertheless,
307 the simulated maximum NPP between the two simulations was identical (5.79 gC m⁻²), although
308 there were regions where simulated NPP was distinctly lower (<3.0 gC m⁻²) under the simulation
309 considering water routing than that ignoring water routing (>3.0 gC m⁻²). Overall, the simulation
310 that neglected water routing had a tendency to overestimate forest NPP in ridges of the
311 watershed or areas with steeper slopes (Fig. 5c).

312 **3.5 Comparison of simulated soil autotrophic and heterotrophic respiration**

313 Simulated monthly-averaged daily soil autotrophic respiration (RA) in July, 1994 ranged
314 from 0.0 to 0.97 gC m⁻² under the simulation with water routing. This range was slightly broader
315 than that from the simulation without water routing, which ranged from 0.35 to 0.97 gC m⁻²

316 (Table 2). When averaged for the entire watershed, monthly average daily soil RA was 8% (0.58
317 vs. 0.63 gC m⁻², Table 2) lower under simulation with water routing than that without water
318 routing. In addition, although the spatial pattern of simulated soil RA across the watershed was
319 extremely similar in most areas between the two simulations (Fig. 6a and 6b), there were patches
320 where simulated soil RA was much lower when water routing was considered (Fig. 6c). Overall,
321 neglect of water routing has the potential to cause R-RHESSys to overestimate soil RA while
322 such overestimates mainly occur in areas of steeper slopes or near the ridges of the watershed
323 (Fig. 6c). Similarly, simulated soil heterotrophic respiration (RH) had a wider range from 0.01 to
324 1.3 gC m⁻² under simulation with water routing and a narrower range from 0.44 to 1.3 gC m⁻²
325 under the simulation without water routing (Table 2). The spatial patterns of simulated soil RH
326 were more variable under simulation with water routing than that without water routing (Fig. 6d
327 and 6e). Besides, when averaged for the entire watershed, monthly average daily soil RH was 11%
328 (0.75 vs. 0.84) lower under the simulation considering water routing than that ignoring water
329 routing. Differing from soil RA, the effects of water routing on soil RH can be either positive or
330 negative when compared to the simulation without water routing (Fig. 6f). The difference in
331 simulated soil RH between the two simulations ranged from -0.8 to 0.12 gC m⁻² across cells.

332 **3.6 Comparison of the differences (with vs. without routing) in monthly values of hydro-**

333 **ecological variables between the “wet” and “dry” scenarios**

334 Fig. 7 shows comparisons of the simulated differences (with vs. without water routing) in
335 monthly values of C and water dynamics in 1995 between the “wet” and “dry” scenarios. When
336 averaged for the entire watershed, the magnitude of the differences in monthly average water
337 table depth and saturation deficit was not distinct for months before July between the two
338 scenarios while the differences diverged for months after July: greater under the “wet” and

339 smaller under the “dry” scenario (Fig. 7a and b). For water fluxes, the absolute magnitude of the
340 differences in monthly transpiration and AET was greater under the “dry” scenario for May, June,
341 July, August, and September, and bottomed in August (Fig. 7d and e). In other months, the
342 magnitude of the differences in monthly transpiration and ET approximated each other between
343 the two scenarios, especially for transpiration (Fig. 7e). However, this pattern of differences in
344 monthly transpiration and AET did not apply to evaporation (Fig. 7c). For C fluxes, the absolute
345 magnitude of the difference in monthly average NPP, soil RA, and RH was greater under the
346 “dry” scenario for May, June, July, August, and September, and bottomed in August (Fig. 7f, g
347 and h). In other months, the simulated differences in the three C fluxes approximated each other
348 between the two scenarios. These results indicated that consideration of water routing has greater
349 effects on simulated water and C dynamics in dry conditions.

350 **4. Discussion**

351 **4.1 Performance and accuracy of R-RHESSys**

352 Our model evaluation against observed streamflow and derived baseflow from the USGS
353 gauge station indicated that R-RHESSys was able to accurately simulate river flow at watershed
354 scales, largely because all algorithms for water, C and nutrient dynamics as well as model
355 parameters are maintained as in RHESSys, which itself has been applied and evaluated in a
356 number of studies (e.g., Christensen et al., 2008; Hwang et al., 2012; Tague and Band, 2001). In
357 addition, the simulated ecological variables – such as LAI and forest NPP– all fell within the
358 ranges of corresponding field observations. For example, modeled LAI during the growing
359 season (May to September) averaged $3.1 \text{ m}^2 \text{ m}^{-2}$ for the entire watershed and ranged from 1.2 to
360 $3.9 \text{ m}^2 \text{ m}^{-2}$ across grid cells, agreeing well with observed and modeled values ranging from 2.90
361 to $4.5 \text{ m}^2 \text{ m}^{-2}$ in mixed oak-hickory forests and northern hardwoods (Scurlock et al., 2001; Tang

362 and Beckage, 2010), dominant forest types in the study watershed. Our modeled annual forest
363 NPP averaged $474 \text{ gC m}^{-2} \text{ yr}^{-1}$, falling within the range of 391 to $574 \text{ gC m}^{-2} \text{ yr}^{-1}$ of field
364 observations in oak-hickories (e.g., Pan et al., 2006; Tang et al., 2010). Nevertheless, we
365 acknowledge that the lack of spatially distributed field measurements – such as observed soil
366 moisture, water table depth, and forest NPP – hinder us in further evaluating the patterns of
367 simulated major ecological and hydrological variables across the watershed. Such limitations in
368 the model's evaluation are encountered commonly in many other distributed-model-based
369 studies (Brooks et al., 2007) and need improvement in the future.

370 **4.2 Effects of water routing on soil water table depth and saturation deficit**

371 Lateral water flow and associated water redistribution across the landscape considerably
372 influence hydrologic response in terrestrial ecosystems, including movement and storage of
373 water in the soil (Guntner and Bronstert, 2004; Thompson and Moore, 1996). Some studies (e.g.,
374 Kim and Eltahir, 2004) indicated that topography drives lateral transport of water downslope,
375 and water converges into concave areas or valleys through surface or subsurface runoff. As a
376 result, water table depth tends to be significantly shallower in valleys compared to hills.
377 However, this contrasting pattern did not occur in simulations that ignored water routing, in
378 which the simulated water table depth and saturation deficit approximated each other between
379 valleys and hills/ridges of the watershed (Fig. 3b and 3e). In other words, simulated water table
380 depth and saturation deficit with water routing captured better our preconception of their spatial
381 patterns across the watershed. A similar study in a humid watershed (Hotta et al., 2010) indicated
382 that lateral flow and local infiltration descending from hillslopes often causes lower elevation
383 sites to have a higher water table level and higher elevation sites to have a lower water table level.

384 A similar model-based comparison study additionally supported our findings. Sonnentag et al.
385 (2008) compared simulated water table depth between simulations with and without considering
386 lateral water flow in a peatland. They found that the magnitude of simulated water table depth
387 without water routing was considerably underestimated because lateral subsurface flow moves
388 water toward the margins of the peat body. The neglect of lateral flow resulted in the simulated
389 water table at or very close to the ground surface, which explains why the simulated water table
390 depth was much greater under simulation ignoring water routing (Table 2). Furthermore, Moore
391 and Thompson (1996) found that the combination of slope curvature, microtopography, and
392 resulting water movement produce significant variability in water table depth across the
393 landscape. This explains why the calculated standard deviation of water table depth among cells
394 doubled (0.40) under simulation considering water routing compared to that (0.19) ignoring
395 water routing (Table 2).

396 Similar to water table depth, saturation deficit under simulation with water routing showed a
397 distinct pattern in the watershed: higher in the valleys and lower in the hills or ridges of the
398 watershed, which agreed better with findings from previous studies. Hopp et al. (2009) found
399 that relatively high saturation in the soil profile occurs in the swale, and drier zone often occurs
400 upslope and on the side ridges of hillslopes when water routing and topography were both
401 considered in the model simulation. Crave and Gascuel-Oudoux (1997) indicated that the steeper
402 upslope parts of a watershed will be drained laterally more rapidly than the gentler downslope
403 parts, resulting in drier slopes at the catchment scale. These patterns were captured by simulation
404 with water routing (Fig. 3d) while not always by simulation without water routing (Fig. 3e). In
405 addition, most previous studies indicated that the upslope contributing area, as incorporated into
406 the TOPMODEL (Beven and Kirkby, 1979), is probably the major topographic influence on soil

407 moisture distribution (e.g., Hotta et al., 2010; Thompson and Moore, 1996). This relationship
408 also was captured better by simulation considering water routing as suggested by the strength of
409 the linear relationship of simulated saturation deficit to calculated topographic wetness index
410 (Fig. 8a vs. 8b) between the two simulations.

411 **4.3 Effects of water routing on water fluxes from land to the atmosphere**

412 Slope, aspect and surrounding topography control incident direct solar radiation, and lower-
413 elevation regions in mountainous watersheds have more incoming longwave radiation from the
414 surrounding landscapes plus temperature decreases as elevation increases. The highest ET values
415 often occur in valleys, and the lowest ET in north-facing, high elevation areas (Bertoldi et al.,
416 2006; Christensen et al., 2008), which explains why the modeled spatial patterns of evaporation
417 and transpiration in the watershed were generally higher in low elevations and valleys and lower
418 in high elevations under the two contrasting simulations (Fig. A3). Water routing is a major
419 determinant of soil water table and moisture distribution, however, both of which play important
420 roles in modulating water fluxes from land to the atmosphere. For example, Salvucci and
421 Entekhabi (1995) indicated that a deeper water table typically indicates drier areas where
422 evaporation is often suppressed. This explains why there are areas where evaporation under
423 simulation with water routing was lower than those without water routing (Fig. A3c).

424 In addition, changes in vegetation growth resulting from moisture alteration also can affect
425 water fluxes from land to the atmosphere due to changes in canopy leaf area. Compared to the
426 two simulations, for cells where simulated NPP decreased (less than -2%, Fig. 5c), 60%
427 experienced an increase in evaporation while 48% experienced a decrease in transpiration due to
428 decrease in canopy leaf area. This explains why there are areas where simulated evaporation is
429 higher while transpiration is lower under simulation with water routing than that without water

430 routing (Fig. A3c and f). At the individual cell level, because temperature, soil moisture and
431 vegetation dynamics interact to jointly control evaporation and transpiration, differences in
432 simulated evaporation, and transpiration can be either positive or negative (Fig. A3). When
433 averaged for the entire watershed, because evaporation showed significant increase by 18%
434 under simulation with water routing, the resultant AET also showed an increase by 9% under
435 simulation with water routing than that without water routing. In addition, because forest
436 productivity is modeled to be similar in 80% of areas between the two simulations and because
437 transpiration accounts for two-thirds of total ET plus water is not limited, simulated transpiration
438 and ET were extremely similar in 70% of areas in the watershed between the two contrasting
439 simulations, although significant differences occurred in some areas (Fig. A3f and i).

440 **4.4 Effects of water routing on vegetation productivity**

441 Changes in soil moisture condition affect canopy photosynthesis and forest productivity
442 (Band et al., 1993). Hwang et al. (2012) found that soil moisture content has profound effects on
443 plant growth in forested watersheds. Svoray and Karnieli (2011) indicated that plant productivity
444 is strongly correlated with water redistribution processes. Plants in the lower physiographic units
445 (e.g., footslope, channel) should respond well to improved water and soil conditions and,
446 therefore, should be more productive. In contrast, the interfluvial, shoulder, and backslope areas
447 often had lower vegetative greenness values because of poor water availability. In this study, the
448 effects of differences in simulated soil moisture condition on forest productivity were not very
449 noticeable (defined as $-2\% < \text{NPP difference} < 2\%$) in 80% of areas in the study watershed between
450 the two contrasting simulations (Fig. 5), largely because incoming solar radiation and
451 temperature are major determinants of forest productivity and these radiative forcings were
452 identical between the two simulations. Nevertheless, because changes in soil moisture can affect

453 forest productivity and because the saturation deficit was simulated to be greater under the
454 simulation with water routing, simulated forest NPP was significantly lower in steeper slope
455 areas of the watershed when water routing was considered. In these areas where differences in
456 NPP were less than -2%, average soil saturation deficit (722 mm) was 45% higher than that (498
457 mm) in areas where differences in NPP were not noticeable (defined as $-2\% < \text{NPP difference} < 2\%$)
458 (Fig. 5). In fact, forest NPP was significantly and negatively correlated with saturation deficit in
459 our simulation (Fig. 9a) because the deterioration of soil moisture condition can limit vegetation
460 growth (e.g., Urgeghe et al., 2010).

461 **4.5 Effects of water routing on soil respiration**

462 Local topography can generate considerable spatial variability in soil temperature, incoming
463 solar radiation, and soil water content (Running et al., 1987; Kang et al. 2004). Although each of
464 these factors differentially affects soil respiration, soil temperature plays a major role in soil
465 respiration. Kang et al. (2004) found that about 75% of seasonal variation in soil respiration in
466 such mesic ecosystems can be explained by variation in soil temperature. Because soil
467 temperature is simulated to be the same between the two simulations, this greatly contributed to
468 the similarity (defined as $-2\% < \text{RA difference} < 2\%$) of the spatial pattern of simulated soil RA in
469 79.9% of areas in the watershed (Fig. 6). Indeed, the calculation of root RA in R-RHESS is
470 mainly treated as a function of soil temperature, following Ryan et al. (1991). Because saturation
471 deficit was higher when water routing was considered, and because soil water deficit limits
472 production of root resulting from reduced NPP, the consequent soil RA is smaller under the
473 simulation considering water routing (Fig. 6a-c). In fact, for cells where simulated NPP
474 decreased by less than -2% between the two contrasting simulations (Fig. 5c), 99.9%

475 experienced a decrease in RA, ranging from -1.4% to -100% (Fig. 6c). Linear regression also
476 suggested that soil RA is negatively and significantly correlated with saturation deficit (Fig. 9b)

477 Although soil temperature plays a dominant role in regulating soil RH, changes in soil water
478 content due to lateral flow and connectivity affect litter production and soil microbial activity,
479 which in turn affect soil RH. les Riveros-Iregui et al. (2011) indicated that growing season soil
480 CO₂ efflux is known to vary laterally by as much as seven-fold within small subalpine
481 watersheds in the northern Rocky Mountains, and the variability was strongly related to the
482 landscape-imposed redistribution of soil water. Because soil RH in R-RHESSys is treated as a
483 function of soil moisture following Parton et al. (1996), this explains that the simulated soil RH
484 is spatially more variable (higher standard deviation) among cells when water routing is
485 considered (Table 2). In our simulation, for cells where forest NPP decreased by less than -2%
486 (Fig. 5c), 97% experienced a decrease in RH due to reduction of litter production (Fig. 6f). In a
487 semiarid subalpine watershed, Riveros-Iregui and McGlynn (2009) observed that the highest soil
488 CO₂ efflux rates often occur in areas with persistently high soil moisture, whereas lower soil CO₂
489 efflux rates are on forested uplands in subalpine watersheds. Such patterns were captured better
490 under simulation considering water routing (Fig. 6d) than that ignoring water routing (Fig. 6e),
491 partially because soil RH was generally simulated to be low in areas of steeper slopes (Figs. 1
492 and 6) and because forest NPP and litter production were low in these areas. Compared to soil
493 RA, differences in simulated soil RH between the two contrasting simulations can be either
494 negative or positive due to combined effects of soil temperature, moisture, and litter inputs on
495 RH. Overall, soil RH was negatively correlated to saturation deficit in our simulation, suggesting
496 that neglect of water routing has potential to cause the model to overestimate soil RH (Fig. 9c).

497 **4.6 Effects of water routing on C and water dynamics under dry conditions**

498 Consideration of water routing in model simulations had greater effects on simulated C and
499 water dynamics under the “dry” scenario than under the “wet” scenario, largely because of
500 deterioration of soil moisture condition under the “dry” scenario (Fig. 10a). For example, when
501 averaged for the entire watershed, soil saturation deficit increased by 14% under the “dry”
502 scenario (0.72 m) compared to the “wet” scenario (0.63 m). The deterioration of soil moisture
503 condition caused the number of cells where the difference in simulated monthly NPP was greater
504 than 2% to increase by 138% under the “dry” scenario (6031 cells) (Fig. 10c) compared to the
505 “wet” scenario (2531 cells, Fig. 10b). This explained why the absolute magnitudes of the
506 simulated differences in monthly values of C and water fluxes were greater for those months, in
507 which time-series of daily precipitation were set as zeroes under the “dry” scenario. Our findings
508 of the greater effects of consideration of water routing on simulated C and water dynamics was
509 consistent with Band (1993), who found that spatial variations in available soil water can have
510 significant effects on areal averaged C and water fluxes rates, particularly under dry conditions.

511 **5. Conclusion**

512 Based on R-RHESSys and by keeping all model parameters and their parameterizations
513 identical, this model-based comparison study indicated the following:

514 (i) R-RHESSys is able to correctly simulate streamflow and baseflow for Biscuit Brook
515 regardless of whether water routing is considered in the model simulation or not. When water
516 routing is considered, however, R-RHESSys captures better our preconception of the spatial
517 patterns of water table depth and saturation deficit. In contrast, when water routing is neglected,
518 the simulation has a tendency to underestimate water table depth and saturation deficit.
519 Simulated patterns of water table depth and saturation deficit differ from our preconception of
520 the two quantities across the landscape.

521 (ii) Differences in simulated water table depth and saturation deficit between simulations
522 with and without water routing affect subsequent water fluxes from land to the atmosphere. At
523 the individual cell level, simulated evaporation, transpiration and ET were spatially more
524 heterogeneous across the landscape when water routing was considered. Although differences in
525 simulated evaporation, plant transpiration, and ET are not significant (absolute difference <2%)
526 in most areas of the watershed, when averaged for the entire watershed, evaporation,
527 transpiration, and ET were simulated to be 4% to 18% greater under simulation considering
528 water routing than that ignoring water routing.

529 (iii) Forest productivity was generally simulated to be smaller and spatially more variable
530 under simulation with water routing due to higher and more variable saturation deficit. Lower
531 forest productivity and root production caused simulated soil RA to be lower when water routing
532 was considered. In contrast, simulated soil RH with water routing can be either greater or smaller
533 than without water routing due to the combined effects of soil moisture, temperature and litter
534 inputs. When averaged for the entire watershed, forest productivity and soil respiration were
535 modeled to be 8% to 11% less under simulation considering water routing than that ignoring
536 water routing.

537 Overall, this study indicated that lateral water flow exerts strong control on the spatial pattern
538 and variability of water table depth and saturation deficit (e.g., Band et al., 1993), and such
539 effects are more apparent in dry conditions (e.g., Band, 1993). When averaged for the entire
540 watershed, simulated water fluxes from land to the atmosphere were higher while forest
541 productivity and soil respiration were less under simulation with water routing than those
542 without water routing. Results of this study further demonstrated that the spatial pattern of soil
543 moisture is fundamental to spatially distributed modeling of eco-hydrological processes (e.g.,

544 Band, 1993; Chamran et al., 2002; Hebrard et al., 2006) and suggested that ecosystem and C
545 cycle models need to explicitly represent water routing because simulation with water routing
546 better captures the patterns of water table depth and saturation deficit across landscapes.

547 **Acknowledgement**

548 The authors thank the New York City Department of Environmental Protection that provided
549 funding for the research that led to this manuscript. We greatly appreciate Dr. Genevieve Ali and
550 other two anonymous reviewers for their constructive comments on earlier version of this
551 manuscript. We sincerely thank Drs. Lawrence Band, Elliot Schneiderman, Don Pierson, and
552 Mark Zion for their valuable comments that greatly helped improve this manuscript. This study
553 also benefited from the NSF EPSCoR grant (NSF 0814372) for Nevada.

554 **References Cited**

- 555 Asbjornsen, H., Goldsmith, G.R., Alvarado-Barrientos, M.S., Rebel, K., Van Osch F.P., Rietkerk,
556 M., Chen, J., Gotsch, S., Tobon, C., Geissert, D.R., Gomez-Tagle, A., Vache, K., Dawson,
557 T.E., 2011. Ecohydrological advances and applications in plant-water relations research: a
558 review. *J. Plant. Ecol.* **4**(1-2), 3-22.
- 559 Band, L.E., 1993. Effects of land surface representation on forest water and carbon budgets. *J.*
560 *Hydrol.* **150**, 749-772.
- 561 Band, L.E., Patterson, P., Nemani, R., Running, S.W., 1993. Forest ecosystem processes at the
562 watershed scale: incorporating hillslope hydrology. *Agr. Forest Meteorol.* **63**, 93-126.
- 563 Bertoldi, G., Rigon, R., Over, T.H., 2006. Impact of watershed geomorphic characteristics on the
564 energy and water budgets. *J. Hydrometeorol.* **7**(3), 389-403.
- 565 Beven, K., Kirkby, M., 1979. A physically-based variable contributing area model of basin
566 hydrology. *Hydrol. Sci. Bull.* **24**(1), 43-69.

567 Brooks, E.S., Boll, J., McDanil, P.A., 2007. Distributed and integrated response of a geographic
568 information system-based hydrologic model in the eastern Palouse region, Idaho. *Hydrol.*
569 *Process.* **21**(1), 110-122.

570 Caylor, K.K., Manfreda, S., Rodriguez-Iturb. 2005. On the coupled geomorphological and
571 ecohydrological organization of river basins. *Adv. Water Resour.* **28**(1), 69-86.

572 Chamran, F., Gessler, P.E., and Chadwick, O.A., 2002. Spatially explicit treatment of soil-water
573 dynamics along a semiarid catena. *Soil Sci. Soc. Am. J.* **66**(5), 1571-1583.

574 Chen, J.M., Chen, X., Ju, W., Geng, X., 2005. Distributed hydrological model for mapping
575 evapotranspiration using remote sensing inputs. *J. Hydrol.* **305**(1-4), 15-39.

576 Christensen, L., Tague, C.L., Baron, J.S., 2008. Spatial patterns of simulated transpiration
577 response to climate variability in a snow dominated mountain ecosystem. *Hydrol. Process.*
578 **22**(18), 3576-3588.

579 Crave, A., Gascuel-Oudou, C., 1997. The influence of topography on time and space distribution
580 of soil surface water content. *Hydrol. Process.* **11**(2), 203-210.

581 Doten, C.O., Bowling, L.C., Lanini, J.S., Maurer, E.P., Lettenmaier, D.P., 2006. A spatially
582 distributed model for the dynamic prediction of sediment erosion and transport in
583 mountainous forested watersheds. *Water Resour. Res.* **42**(4). W04417,
584 doi:10.1029/2004WR003829.

585 Gerard-Marchanti, P., Hively, W.D., Steenhuis, T.S., 2006. Distributed hydrological modelling
586 of total dissolved phosphorus transport in an agricultural landscape, part I: distributed runoff
587 generation. *Hydrol. Earth Syst. Sci.* **10**(2), 245-261.

588 Goovaerts, P., 1998. Ordinary cokriging revisited. *Math. Geol.* **30**, 21-42.

589 Guntner, A., Bronstert, A., 2004. Representation of landscape variability and lateral
590 redistribution processes for large-scale hydrological modelling in semi-arid areas. *J. Hydrol.*
591 **297**(1-4), 136-161.

592 Hebrard, O., Voltz, M., Andrieux, P., Moussa, R., 2006. Spatio-temporal distribution of soil
593 surface moisture in a heterogeneously farmed Mediterranean catchment. *J. Hydrol.* **329**(1-2),
594 110-121.

595 Hopp, L., Harman, C., Desilets, S.L.E., Graham, C.B., McDonnell, J.J., Troch, P.A., 2009.
596 Hillslope hydrology under glass: confronting fundamental questions of soil-water-biota co-
597 evolution at Biosphere 2. *Hydrol. Earth Syst. Sci.* **13**(11), 2105-2118.

598 Hotta, N., Tanaka, N., Sawano, S., Kuraji, K., Shiraki, K., Suzuki, M., 2010. Changes in
599 groundwater level dynamics after low-impact forest harvesting in steep, small watersheds. *J.*
600 *Hydrol.* **385**(1-4), 120-131.

601 Hwang, T., Band, L.E., Vose, J.M., Tague, C., 2012. Ecosystem processes at the watershed scale:
602 Hydrologic vegetation gradient as an indicator for lateral hydrologic connectivity of
603 headwater catchments. *Water Resour. Res.* **48**. doi:10.1029/2011WR011301.

604 Ivanov, V.Y., Bras, R.L., Vivoni, E.R., 2008. Vegetation-hydrology dynamics in complex terrain
605 of semiarid areas: 2. Energy-water controls of vegetation spatiotemporal dynamics and
606 topographic niches of favorability. *Water Resour. Res.* **44**(3). W03430,
607 doi:10.1029/2006WR005595.

608 Ju, W., Chen, J.M., Black, A.B., Barr, A.G., McCaughey, H., Roulet, N.T., 2006. Hydrological
609 effects on carbon cycles of Canada's forests and wetlands. *Tellus B* **58**(1), 16-30.

610 Kang, S., Lee, D., Kimball, J.S., 2004. The effects of spatial aggregation of complex topography
611 on hydro-ecological process simulations within a rugged forest landscape: development and
612 application of a satellite-based topoclimatic model. *Can. J. For. Res.* 34(3), 519–530

613 Kim, Y., Eltahir, E.A.B., 2004. Role of topography in facilitating coexistence of trees and
614 grasses within savannas. *Water Resour. Res.* **40**(7). W07505, doi:10.1029/2003WR002578.

615 Lane, S.N., Reaney, S.M., Heathwaite, A.L., 2009. Representation of landscape hydrological
616 connectivity using a topographically driven surface flow index. *Water Resour. Res.* **45**,
617 W08423, doi:10.1029/2008WR007336.

618 Mahmood, T.H., Vivoni, E.R., 2011. A climate-induced threshold in hydrologic response in a
619 semiarid ponderosa pine hillslope. *Water Resour. Res.* **47**. W09529,
620 doi:10.1029/2011WR010384.

621 Moore, R.D., Thompson, J.C., 1996. Are water table variations in a shallow forest soil consistent
622 with the TOPMODEL concept? *Water Resour. Res.* **32**(3), 663-669.

623 Nash, J. E., Sutcliffe, J.V., 1970. River flow forecasting through conceptual models part I – A
624 discussion of principles, *J. Hydrol.* **10**, 282–290.

625 Pan, Y., Birdsey, R., Hom, J., McCullough, K., Clark, K., 2006. Improved estimates of net
626 primary productivity from MODIS satellite data at regional and local scales. *Ecol. Appl.* **16**,
627 125–132.

628 Parton, W.J., Mosier, A.R., Ojima, D.S., Valentine, D.W., Schimel, D.S., Weier, K., Kulmala,
629 A.E., 1996. Generalized model for N₂ and N₂O production from nitrification and
630 denitrification. *Global Biogeochem. Cy.* **10**(3), 401-412.

631 Pockman, W.T., Small, E.E., 2010. The Influence of Spatial Patterns of Soil Moisture on the
632 Grass and Shrub Responses to a Summer Rainstorm in a Chihuahuan Desert Ecotone.
633 *Ecosystems* **13**(4), 511-525.

634 Price, M.F., Gratzner, G., Duguma, L.A., Kohler, T., Maselli, D., Romeo, R.(editors) 2011.
635 *Mountain Forests in a Changing World - Realizing Values, addressing challenges*. Published
636 by FAO/MPS and SDC, Rome.

637 Quinn, P., Beven, K., Chevallier, P., Planchon, O., 1991. The prediction of hillslope flow paths
638 for distributed hydrological modeling using digital terrain models. *Hydrol. Proc.* **5**, 59–79.

639 Ridolfi, L., D'Odorico, P., Porporato, A., Rodriguez-Iturbe, I., 2003. Stochastic soil moisture
640 dynamics along a hillslope. *J. Hydrol.* **272**(1-4), 264-275.

641 Riveros-Iregui, D.A., McGlynn, B.L., 2009. Landscape structure control on soil CO₂ efflux
642 variability in complex terrain: Scaling from point observations to watershed scale fluxes. *J.*
643 *Geophys. Res.-Biogeo.* **114**. G02010, doi:10.1029/2008JG000885.

644 Riveros-Iregui, D.A., McGlynn, B.L., Marshall, L.A., Welsch, D.L., Emanuel, R.E., Epstein,
645 H.E., 2011. A watershed-scale assessment of a process soil CO₂ production and efflux model.
646 *Water Resour. Res.* **47**. W00J04, doi:10.1029/2010WR009941.

647 Running, S.W., Nemani, R.R., Hungerford, R.D., 1987. Extrapolation of Synoptic
648 Meteorological Data in Mountainous Terrain and Its Use for Simulating Forest
649 Evapotranspiration and Photosynthesis. *Can. J. Forest Res.* **17**(6), 472-483.

650 Ryan, M.G., 1991. Effects of climate change on plant respiration. *Ecol. Appl.* **1**(2), 157-167.

651 Salvucci, G.D., Entekhabi, D., 1995. Hillslope and Climatic Controls on Hydrologic Fluxes.
652 *Water Resour. Res.* **31**(7), 1725-1739.

653 Scurlock, J.M.O., Asner, G.P., Gower, S.T., 2001. Global Leaf Area Index from Field
654 Measurements, 1932-2000. Data source: Oak Ridge National Laboratory Distributed Active
655 Archive Center, Oak Ridge, Tennessee, USA. (<http://www.daac.ornl.gov>)

656 Singh, R., Jhorar, R.K., van Dam, J.C., Feddes, R.A., 2006. Distributed ecohydrological
657 modelling to evaluate irrigation system performance in Sirsa district, India II: Impact of
658 viable water management scenarios. *J. Hydrol.* **329**(3-4), 714-723.

659 Smith, M.B., Koren, V., Reed, S., Zhang, Z., Zhang, Y., Moreda, F., Cui, Z., Naoki, M.,
660 Anderson, E.A., Cosgrove, B.A., 2012. The distributed model intercomparison project -
661 Phase 2: Motivation and design of the Oklahoma experiments. *J. Hydrol.* **418-419** (2012), 3-
662 16.

663 Smith, M.W., Bracken, L.J., Cox, N.J., 2010. Toward a dynamic representation of hydrological
664 connectivity at the hillslope scale in semiarid areas. *Water Resour. Res.* **46**. W12540,
665 doi:10.1029/2009WR008496.

666 Sonntag, O., Chen, J.M., Roulet, N.T., Ju, W., Govind, A., 2008. Spatially explicit simulation
667 of peatland hydrology and carbon dioxide exchange: Influence of mesoscale topography. *J.*
668 *Geophys. Res.-Biogeo.* **113**(G2). DOI: 10.1029/2007JG000605.

669 Sponseller, R.A., Fisher, S.G., 2008. The influence of drainage networks on patterns of soil
670 respiration in a desert catchment. *Ecology* **89**(4), 1089-1100.

671 Svoray, T., Karnieli, A., 2011. Rainfall, topography and primary production relationships in a
672 semiarid ecosystem. *Ecohydrology* **4**(1), 56-66.

673 Tague, C.L., Band, L.E., 2001. Evaluating explicit and implicit routing for watershed hydro-
674 ecological models of forest hydrology at the small catchment scale. *Hydrol. Process.* **15**(8),
675 1415-1439.

676 Tague, C.L., Band, L.E., 2004. RHESSys: regional hydro-ecologic simulation system – an
677 objected-oriented approach to spatially distributed modeling of carbon, water and nutrient
678 cycling. *Earth interact.* **8**, 1–42.

679 Tang, G., Arnone III, J., 2013. Trends in surface air temperature and temperature extremes in the
680 Great Basin during the 20th century from ground-based observations. *J. Geophys. Res.–*
681 *Atmos.* **118**, 3579-3589.

682 Tang, G., Beckage, B., 2010. Projecting the distribution of forests in New England in response to
683 climate change. *Divers. Distrib.* **16**, 144-158.

684 Tang, G., Beckage, B., Smith, B., Miller, P.A., 2010. Estimating potential forest NPP, biomass
685 and their climatic sensitivity in New England using a regional dynamic ecosystem model.
686 *Ecosphere* 1(6), 1–20 (Article 18).

687 Thompson, J.C., Moore, R.D., 1996. Relations between topography and water table depth in a
688 shallow forest soil. *Hydrol. Process.* **10**(11), 1513-1525.

689 Thompson, S., Katul, G., Konings, A., Ridolfi, L. 2011. Unsteady overland flow on flat surfaces
690 induced by spatial permeability contrasts. *Adv. Water Resour.* **34**(8), 1049-1058.

691 Urgeghe, A.M., Breshears, D.D., Martens, S.N., Beeson, P.C., 2010. Redistribution of Runoff
692 Among Vegetation Patch Types: On Ecohydrological Optimality of Herbaceous Capture of
693 Run-On. *Rangeland Ecol. Manag.* **63**(5), 497-504.

694 Vogelmann, J.E., Sohl, T., Campbell, P.V., Shaw, D.M., 1998a. Regional land cover
695 characterization using landsat thematic mapper data and ancillary data sources. *Environ.*
696 *Monit. Assess.* **51**, 415–428

697 Vogelmann, J.E., Sohl, T., Howard, S.M., 1998b. Regional characterization of land cover using
698 multiple sources of data. *Photogramm. Eng. Remote. Sens.* **64**, 45–47

699 Wang, J.H., Yang, H., Li, L., Gourley, J. J., Sadiq, I. K., Yilmaz, K. K., Adler, R. F., Policelli, F.
700 S., Habib, S., Irwn, D., Limaye, A. S., Korme, T. & Okello, L., 2011. The coupled routing
701 and excess storage (CREST) distributed hydrological model. *Hydrol. Sci. J.* **56**(1), 84-98.

702 Wang, L., Koike, T., Yang, K., Jackson, T.J., Bindlish, R., Yang, D., 2009. Development of a
703 distributed biosphere hydrological model and its evaluation with the Southern Great Plains
704 Experiments (SGP97 and SGP99). *J. Geophys. Res.-Atmos.* **114**. D08107,
705 doi:10.1029/2008JD010800

706 Wigmosta, M., Vail, L., Lettenmaier, D., 1994. Distributed hydrology–vegetation model for
707 complex terrain. *Water Resour. Res.* **30**, 1665–1679.

708

709

710 **Tables**711 **Table 1.** Major soil parameters and their parameterizations used in this study

Variables	Unit	Soil texture			
		Sandy loam	Silt loam	Loamy skeleton	Rocky
$K_{sat_0}^\dagger$	m day ⁻¹	89.05	48.62	48.36	109.56
m^\dagger	DIM	0.09	0.12	0.13	0.09
Porosity	%	0.435	0.410	0.451	0.485
Porosity decay	DIM	4000	4000	4000	4000
Pore size index (PSI)	DIM (0-1)	0.204	0.189	0.186	0.228
PSI air entry	%	0.218	0.386	0.478	0.480
Soil depth	m	5.0	5.2	4.8	5.0
Active zone depth	m	10	10.0	10.0	10.0
Maximum energy capacity	°C	-10.	-10.	-10.	-10.
Albedo	DIM	0.258	0.253	0.320	0.200
Sand	%	0.70	0.20	0.80	0.75
Clay	%	0.10	0.15	0.02	0.05
Silt	%	0.20	0.65	0.18	0.20

712 [†] K_{sat_0} is saturated hydraulic conductivity at the surface; m is the decay rate of hydraulic conductivity with depth.713 K_{sat_0} and m were manually calibrated against observed streamflow and derived baseflow at the USGS gauge station.

714

715 **Table 2.** Comparison of simulated hydrological and ecological variables between the two

716 contrasting simulations: with vs. without water routing

Variables	Water routing	Minimum	Maximum	Mean	STD
Water table depth (m)	Yes	0.15	2.92	1.20	0.40
	No	0.02	1.20	0.72	0.19
Saturation deficit (m)	Yes	0.08	1.42	0.54	0.17
	No	0.01	0.54	0.33	0.08
Evaporation (mm)	Yes	0.22	3.11	0.87	0.42
	No	0.52	1.05	0.74	0.05
Plant transpiration (mm)	Yes	0.00	3.86	1.41	0.49
	No	0.92	1.95	1.35	0.13
Evapotranspiration (mm)	Yes	0.28	6.65	2.27	0.79
	No	1.44	2.99	2.09	0.18
NPP (gC m ⁻² day ⁻¹)	Yes	0.01	5.79	3.33	0.84
	No	2.50	5.79	3.60	0.17
RA (gC m ⁻² day ⁻¹)	Yes	0.00	0.97	0.58	0.18
	No	0.35	0.97	0.63	0.08
RH (gC m ⁻² day ⁻¹)	Yes	0.01	1.3	0.75	0.20
	No	0.44	1.3	0.84	0.08

717 **Figure Captions**

718 **Fig. 1.** The location of the Biscuit Brook watershed (red area) and the United States Geological
719 Survey gauge station within the Catskill Mountain region of New York state. The map on the left
720 depicts boundaries of the West of Hudson watershed and reservoirs of the New York City water
721 supply system. The black points are ten Cooperative Observer Program weather stations used to
722 derive meteorological data for the watershed.

723

724 **Fig. 2.** Calibration (for the period 1/1/1992 – 12/31/1993) and evaluation (for the period
725 1/1/1994 – 12/31/1995) of R-RHESSys simulated daily streamflow (SF) and baseflow (BF) (solid
726 red line) against observed/derived data (solid black line). Simulations in (a) and (b) considered
727 water routing while simulations in (c) and (d) ignored water routing. NS is short for the Nash-
728 Sutcliff coefficient. The blue-dashed line represents January 1, 1994.

729

730 **Fig. 3.** Comparison of simulated monthly average daily soil water table depth and saturation
731 deficit in July, 1994 between the two contrasting simulations: (a) and (d) considered water
732 routing while (b) and (e) ignored water routing. (c) and (f) show differences in simulated soil
733 water table depth and saturation deficit between the two contrasting simulations.

734

735 **Fig. 4.** Comparison of simulated monthly average daily evaporation (evap), transpiration (Tran),
736 and actual evapotranspiration (AET) in July, 1994 between the two simulations with and without
737 (indicated by “NO”) consideration of water routing.

738

739 **Fig. 5.** Comparison of simulated monthly average daily net primary productivity (NPP) in July,
740 1994 between the two simulations: (a) considering water routing and (b) ignoring water routing.
741 (c) shows percentage difference between (a) and (b) divided by the result from simulation (a)
742 considering water routing. The white areas show no significant differences.

743

744 **Fig. 6.** Comparison of simulated monthly average daily soil autotrophic (RA) and heterotrophic
745 respiration (RH) in July, 1994 between the two simulations: (a) and (d) considering water routing
746 while (b) and (e) ignoring water routing. (c) and (f) show percentage differences between the two
747 simulations divided by results from the simulation considering water routing. The white areas
748 show no significant differences.

749

750 **Fig. 7.** Comparison of the simulated differences (with vs. without water routing) in monthly
751 values of major hydro-ecological variables between the “wet” (solid black line) and “dry” (solid
752 red line) scenarios.

753

754 **Fig. 8.** Comparison of the relationships of simulated saturation deficit (SD) to topographic
755 wetness index (TWI) across the watershed between the two simulations: (a) considering water
756 routing and (b) ignoring water routing.

757

758 **Fig. 9.** The relationships of saturation deficit (SD) with net primary productivity (NPP), (b) soil
759 autotrophic respiration (RA), and (c) soil heterotrophic respiration (RH). Data shown here are
760 based on the simulation considering water routing.

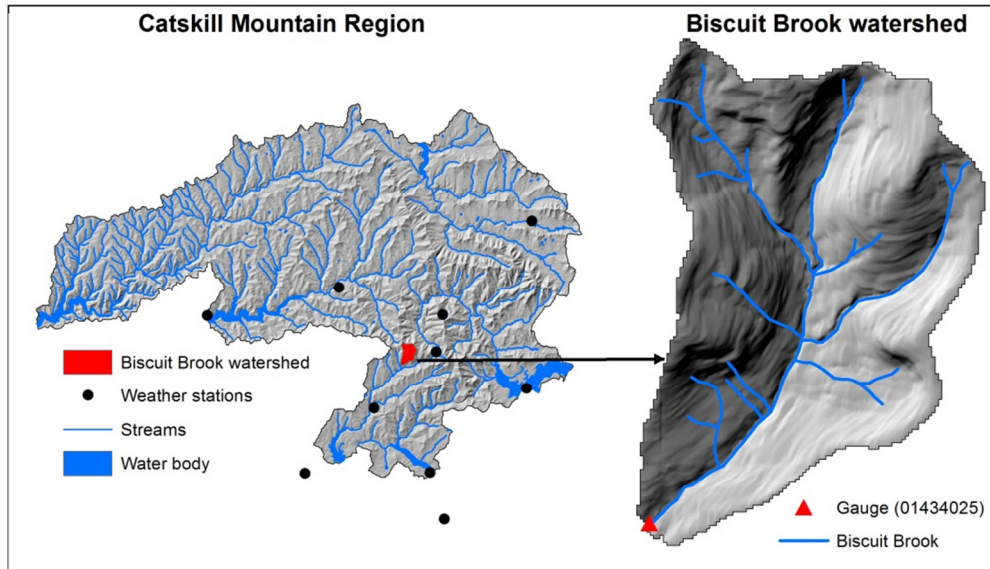
761

762 **Fig. 10.** (a) Deterioration of soil moisture condition under the “dry” scenario compared to the
763 “wet” scenario resulted in NPP decreases occurring in more areas of the watershed (c) under the
764 “dry” scenario than that (b) under the “wet” scenario. The white areas show no significant
765 differences.

766

767 **Figures**

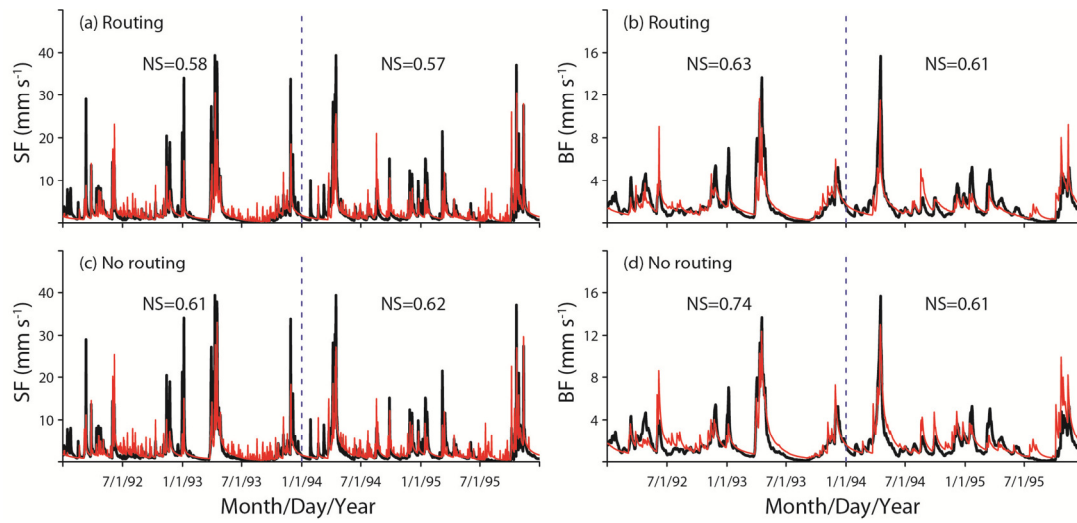
768 **Fig. 1.**



769

770

771 **Fig. 2.**



772

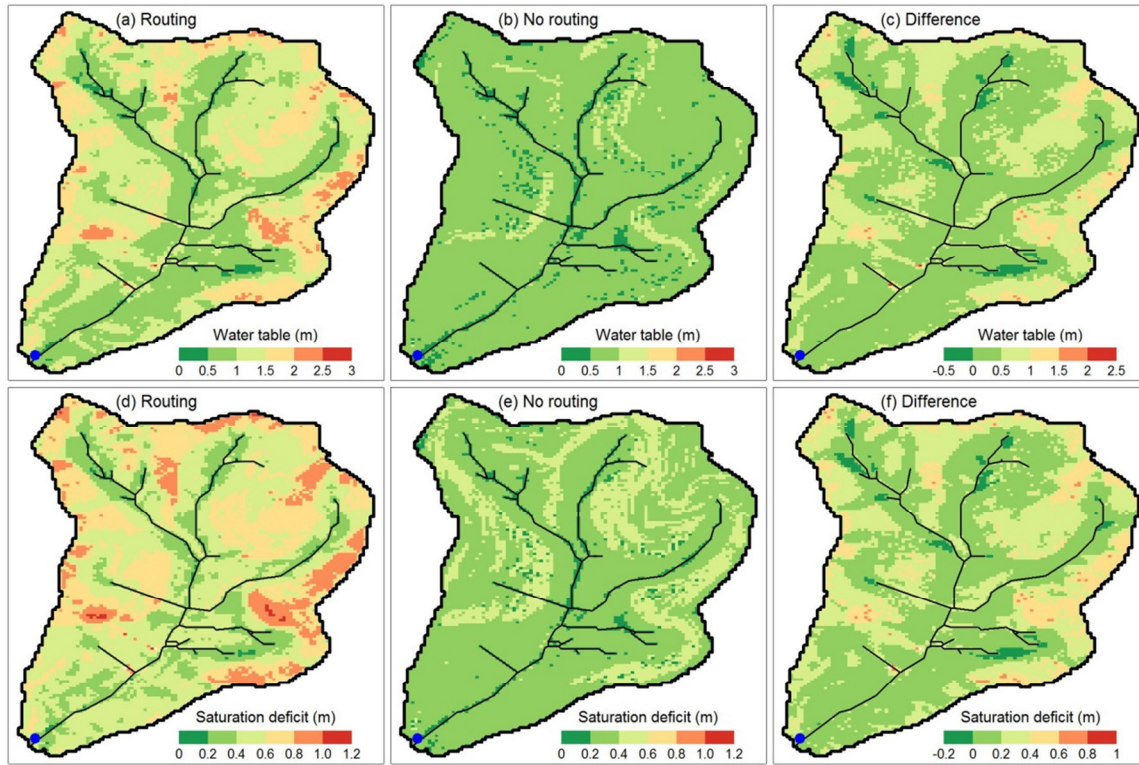
773

774

775

776

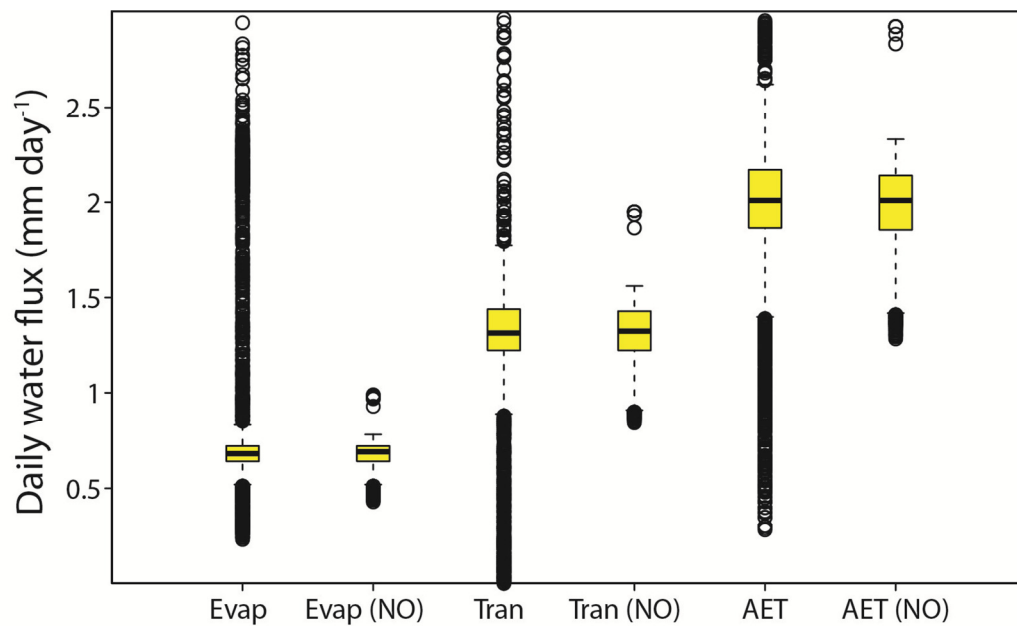
777 **Fig. 3.**



778

779

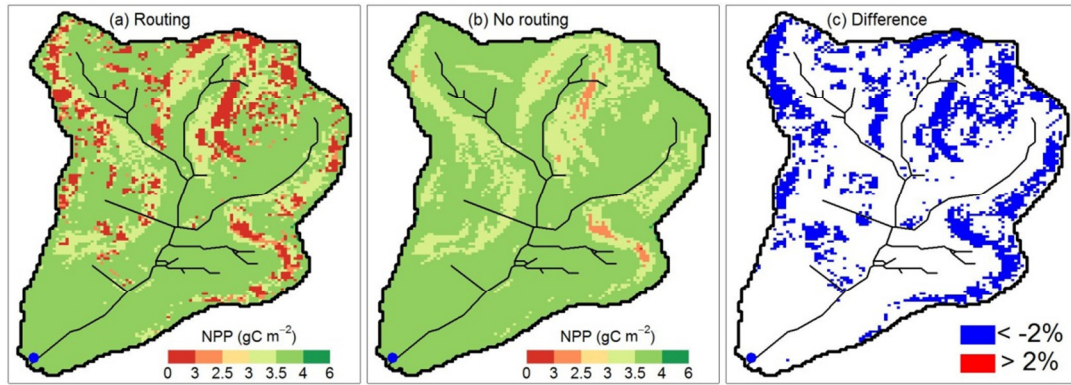
780 **Fig. 4.**



781

782

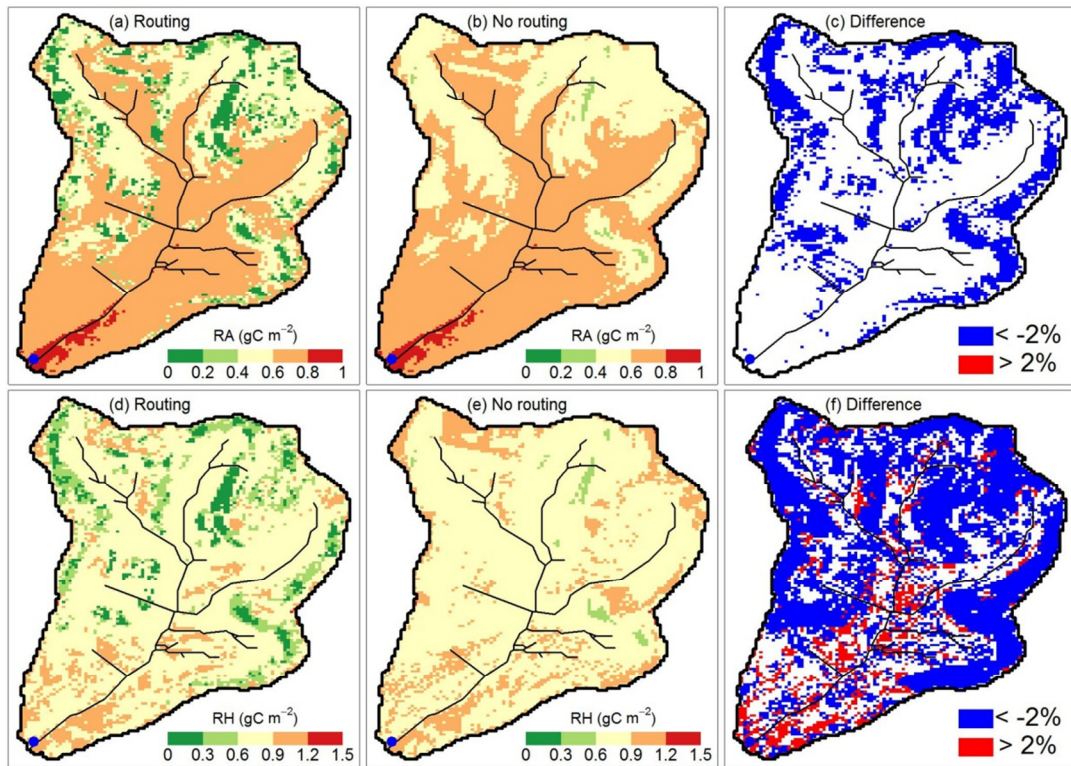
783 **Fig. 5.**



784

785

786 **Fig. 6.**



787

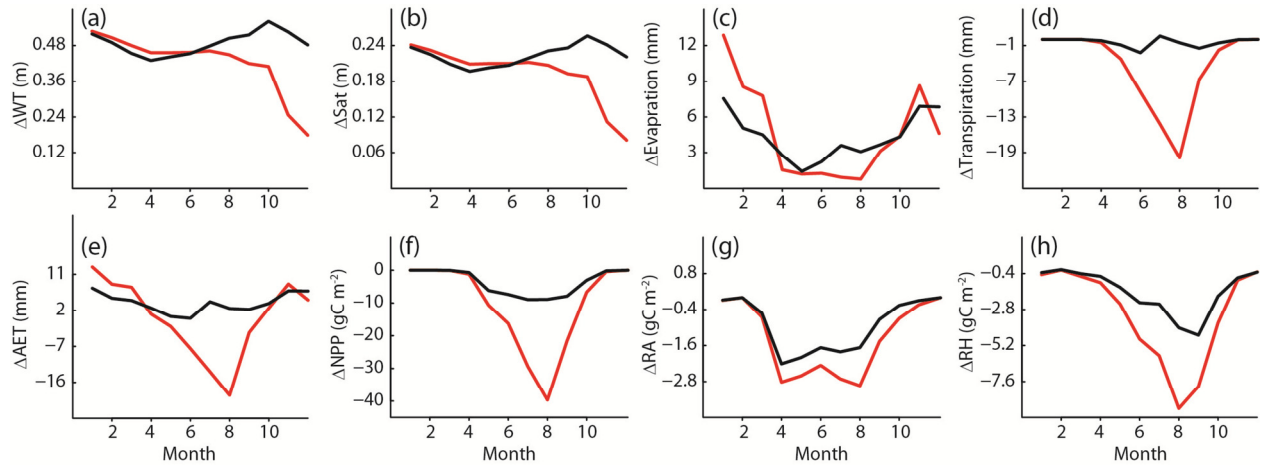
788

789

790

791

792 **Fig. 7.**

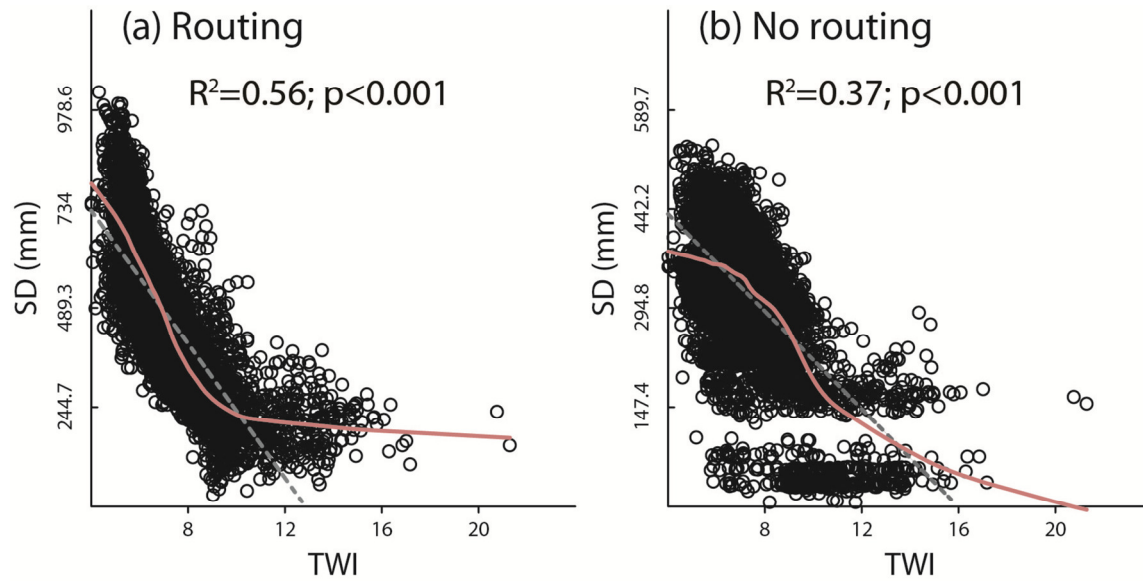


793

794

795

796 **Fig. 8.**



797

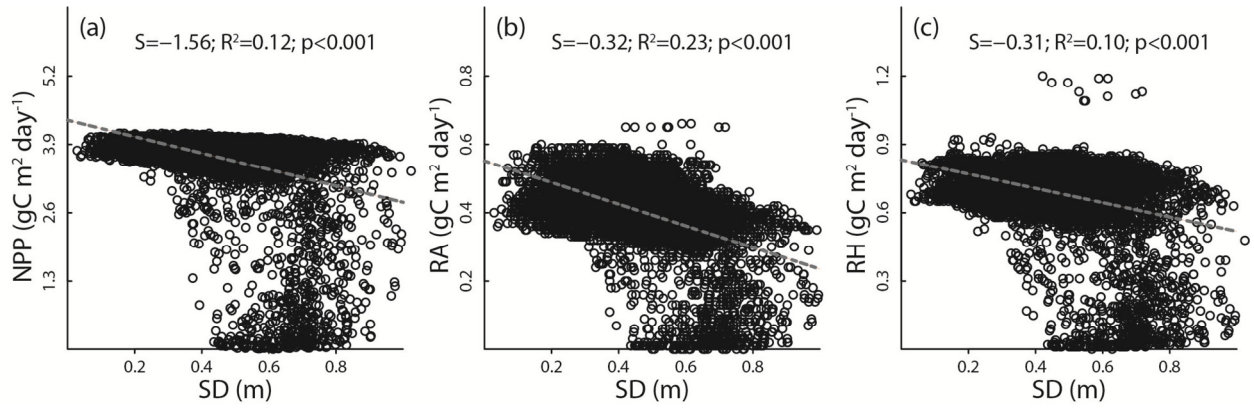
798

799

800

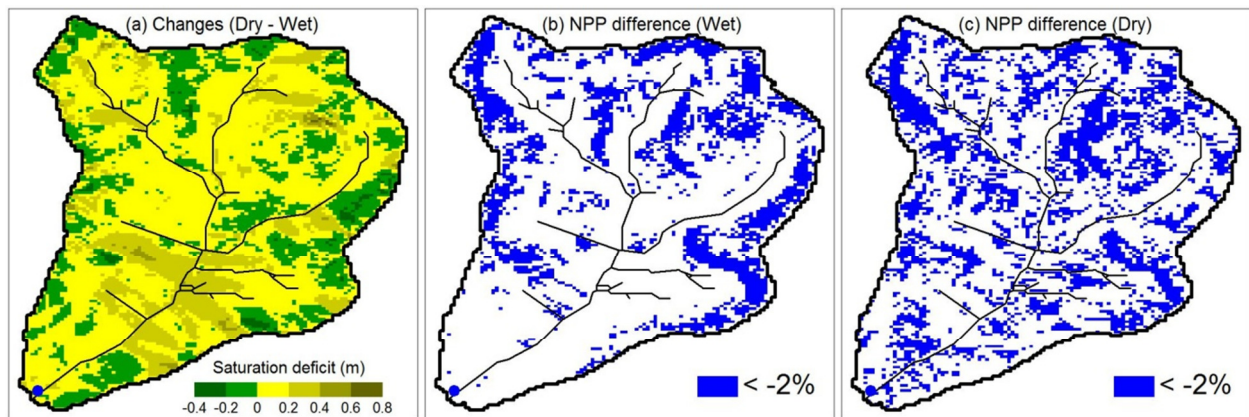
801

802 **Fig. 9.**



803

804 **Fig. 10.**



805

806